Available online at www.sciencedirect.com
ScienceDirect
Advances in Water Resources 31 (2008) 339–354
Advances in Water Resources
www.elsevier.com/locate/advwatres

Effects of pore-scale dispersion, degree of heterogeneity, sampling size, and source volume on the concentration moments of conservative solutes in heterogeneous formations

Daniele Tonina [a,*], Alberto Bellin [b]

[a] *Daniele Tonina, University of California Berkeley, and at USFS Rocky Mountain Research Station Boise, 322 East Front Street, Suite 401, Boise ID 83702, United States*

[b] *Alberto Bellin, Dipartimento di Ingegneria Civile ed Ambientale, Università di Trento, via Mesiano 77, I-38050 Trento, Italy*

Received 23 March 2007; received in revised form 17 July 2007; accepted 28 August 2007
Available online 4 September 2007

Abstract

Pore-scale dispersion (PSD), aquifer heterogeneity, sampling volume, and source size influence solute concentrations of conservative tracers transported in heterogeneous porous formations. In this work, we developed a new set of analytical solutions for the concentration ensemble mean, variance, and coefficient of variation (CV), which consider the effects of all these factors. We developed these models as generalizations of the first-order solutions in the log-conductivity variance of point concentration proposed by [Fiori A, Dagan G. Concentration fluctuations in aquifer transport: a rigorous first-order solution and applications. J Contam Hydrol 2000;45(1–2):139–163]. Our first-order solutions compare well with numerical simulations for small and moderate formation heterogeneity and from small to large sampling and source volumes. However, their performance deteriorates for highly heterogeneous formations. Successively, we used our models to study the interplay among sampler size, source volume, and PSD. Our analysis shows a complex and important interaction among these factors. Additionally, we show that the relative importance of these factors is also a function of plume age, of aquifer heterogeneity, and of the measurement location with respect to the mean plume center of gravity. We found that the concentration moments are chiefly controlled by the sampling volume with pore-scale dispersion playing a minor role at short times and for small source volumes. However, the effect of the source volume cannot be neglected when it is larger than the sampling volume. A different behavior occurs for long periods, which may be relevant for old contaminations, or for small injection volumes. In these cases, PSD causes a significant dilution, which is reflected in the concentration statistics. Additionally, at the center of the mean plume, where high concentrations are most likely to occur, we found that sampling volume and PSD are attenuating mechanisms for both concentration ensemble mean and coefficient of variation, except at very large source and sampler sizes, where the coefficient of variation increases with sampler size and PSD. Formation heterogeneity causes a faster reduction of the ensemble mean concentrations and a larger uncertainty at the center of the mean plume. Therefore, our results highlight the importance of considering the combined effect of formation heterogeneity, exposure volume, PSD, source size, and measurement location in performing risk assessment.

Keywords: Solute transport; Groundwater; Concentration moments; Stochastic methods

1. Introduction

A great effort has been spent in the last few decades for better understanding the spatial and temporal evolution of solute concentrations in heterogeneous porous formations. Important advances have been obtained in this field mostly considering point concentrations, which are defined over a

* Corresponding author. Tel.: +1 208 3734381; fax: +1 208 3734391.
E-mail addresses: dtonina@berkeley.edu (D. Tonina), Alberto.Bellin@unitn.it (A. Bellin).

0309-1708/$ - see front matter © 2007 Elsevier Ltd. All rights reserved.
doi:10.1016/j.advwatres.2007.08.009

small but finite volume of size ℓ. According to the continuum approach to flow in porous formations ℓ should be smaller than the typical scale of variability of the hydraulic conductivity (I_Y), but large enough to define macroscopic quantities such as porosity and hydraulic conductivity (see e.g., [3], ch. 1). Hence, when this property is satisfied, the continuum approach applies at scales larger than ℓ and point values of physical quantities can be defined and treated with the mathematical machinery of continuum theory (see e.g., [2], ch. 1). However, a large disparity of sampling volumes, whose dimensions depend on the way concentrations are measured, is observed in applications. For instance, solute concentrations are usually measured in observation wells, spanning several vertical integral scales of the log-conductivity, or in the effluent of extraction wells, with a sampling volume that can be approximated by their capture zone for continuous, or long-lasting, extractions. Therefore, point measurements are rare and the characteristic size of the sampling volume is typically much larger than ℓ. In these cases, besides dilution associated with pore-scale dispersion (PSD), which mixes solute at scales smaller than ℓ, measured solute concentrations are influenced by mixing of solute mass within the sampling volume.

An important case in which attenuation of solute concentrations associated with the sampling volume should be carefully evaluated is risk assessment, because sampling volume influences solute concentrations dramatically at the exposure location. For instance, sampling volumes vary if risk analysis of exposure to a contaminant is assessed in a drinking water distribution system at the production well or at the in-house taps. In the former case, the sampling volume would be the volume of the well, whereas in the latter case, a reasonable choice would be the aquifer volume within the well capture zone with travel time less or equal to the turnover time, $t_r = V_r/Q$, of the storage facility, whose volume is V_r, and Q is the mean water discharge extracted from the well. In both cases, the level of exposure depends critically on the interplay between the spatial distribution of the solute mass within the aquifer and the size of the sampling volume.

The impact of the sampling volume on the first two moments of the solute concentration has been investigated by Andričević [1], who concluded that whereas both PSD and sampling volume attenuate solute concentrations, their relative importance depends on the elapsed time since injection. In his derivation, he utilized closures developed in solute transport in turbulent flows to quantify the correlation terms between concentration and velocity fields and a number of additional assumptions in order to illustrate qualitatively the impact of the sampling volume on the concentration variance. In particular, he computed the concentration variance by integrating, over the sampling volume, the product of the variance of the point concentration and the correlation function. The former has been assumed constant over the sampling volume and the latter has been assumed to decrease exponentially with the two-point separation distance (see Eqs. (33), (34) and (35) of [1]). However, these solutions have been utilized by Andričević to study the impact of the sampling volume qualitatively on solute concentration, and they cannot be used as a predictive tool in risk assessment because of the many assumptions he adopted.

To overcome this difficulty and to further explore the impact of PSD and sampling volume on the concentration moments, we developed new first-order solutions of the first two moments of volume-averaged solute concentrations. We started our development from the first-order solutions obtained by Fiori and Dagan [12] for the first and second moments of point solute concentrations in heterogeneous aquifers. In the remaining sections, first we generalize these solutions to include the effect of the sampling volume ΔV and then, after a thorough testing with accurate numerical simulations, we use them to analyze the effect of ΔV, source size, and PSD on the moments of solute concentrations.

2. First-order solutions for solute concentrations

Let us consider a tracer of constant concentration C_0 released instantaneously within the volume V_0, and assume that the total mass $M_0 = n\ V_0 C_0$ is subdivided into N_p non-interacting particles, each of them with the elementary mass $\Delta m = n\ C_0\ V_0/N_p$, where n indicates the formation's porosity, which is considered constant through the aquifer (e.g., [7,14,16]). The point concentration $C(\mathbf{x},t)$ expresses the mass of solute per unit volume of fluid contained into an elementary infinitesimal volume ($\Delta V \to 0$) centered at $\mathbf{x}$:

$$C(\mathbf{x},t) = \int_{V_0} \mathrm{d}\mathbf{a} C_0(\mathbf{a}) \delta[\mathbf{x} - \mathbf{X}_t(t;\mathbf{a})] \tag{1}$$

where δ is the Dirac delta function, and $\mathbf{X}_t(t;\mathbf{a})$ is the trajectory of the particle released at position $\mathbf{x} = \mathbf{a}$ within V_0:

$$\mathbf{x} = \mathbf{X}_t(t;\mathbf{a}) = \widetilde{\mathbf{X}}(t;\mathbf{a}) + \mathbf{X}_b \tag{2}$$

Following Fiori and Dagan [12] in Eq. (2) the particle trajectory has been split into two components: the advective displacement $\widetilde{\mathbf{X}}$, which in principle can be obtained by solving the following integro-differential equation $\mathrm{d}\widetilde{\mathbf{X}}(t)/\mathrm{d}t = \mathbf{v}[\mathbf{X}_t(t)]$, where $\mathbf{v}$ is the local velocity, and the Brownian component $\mathbf{X}_b$. The latter is a Wiener process with zero mean and variance matrix $X_{b,ii}(t) = 2D_{d,ii}t$ resulting from a constant diagonal dispersion tensor $D_{d,ii} = \alpha_{ii}|\mathbf{U}|$, $i = 1, \ldots, N$ [1,12,20]. In the last two expressions, N is the space dimensionality, α_{ii} is the pore-scale dispersivity, and $\mathbf{U}$ is the aquifer mean velocity, which for simplicity, but without lack of generality, is assumed aligned with the x_1 direction. The Brownian motion is introduced to model pore-scale dispersion, a process occurring at a scale smaller than ℓ, and from Eq. (2) can be expressed as the difference between the particle trajectory and the advective displacement ($\mathbf{X}_b = \mathbf{X}_t - \widetilde{\mathbf{X}}$).

We define the resident concentration $C_{\Delta V}$ for a volume ΔV centered at $\mathbf{x}$ as the solute mass per unit of volume that at time t is within ΔV:

$$C_{\Delta V}(\mathbf{x},t)=\frac{1}{\Delta V}\int_{\Delta V}\mathrm{d}\mathbf{x}\int_{V_0}\mathrm{d}\mathbf{a}C_0(\mathbf{a})\delta[\mathbf{x}-\mathbf{X}_t(t;\mathbf{a})] \tag{3}$$

Accepting that a detailed mapping of the formation hydraulic properties cannot be obtained, we model the log-conductivity $Y=\ln(K)$, where K is the local hydraulic conductivity, as a stationary random space function (RSF). Consequently to this choice, solute concentration $C_{\Delta V}$ is also modeled as a RSF with probability density function that depends on the statistical properties of Y, through flow and transport equations.

The ensemble mean of $C_{\Delta V}$ is obtained by taking the statistical expectation of Eq. (3):

$$\langle C_{\Delta V}(\mathbf{x},t)\rangle=\frac{1}{\Delta V}\int_{\Delta V}\mathrm{d}\mathbf{x}\int_{V_0}\mathrm{d}\mathbf{a}C_0(\mathbf{a})\int\mathrm{d}\widetilde{\mathbf{X}}\int\mathrm{d}\mathbf{X}_b\times\delta[\mathbf{x}-\widetilde{\mathbf{X}}(t;\mathbf{a})-\mathbf{X}_b]f(\widetilde{\mathbf{X}},\mathbf{X}_b) \tag{4}$$

where $f(\widetilde{\mathbf{X}},\mathbf{X}_b)$ is the pdf of the particle trajectory. Because of the particle trajectory splitting into advective and Brownian components, f coincides with the multivariate joint pdf of $\widetilde{\mathbf{X}}$ and $\mathbf{X}_b$, which, according to the Bayes rule, is given by the product of the marginal pdf of $\widetilde{\mathbf{X}}$ and the pdf of $\mathbf{X}_b$ conditional to $\widetilde{\mathbf{X}}$: $f(\widetilde{\mathbf{X}},\mathbf{X}_b)=\varphi\prime(\widetilde{\mathbf{X}})\varphi_C(\mathbf{X}_b\mid\widetilde{\mathbf{X}})$. Fiori and Dagan [12] showed that at the first-order of approximation in σ_Y^2, advective and Brownian components of the total displacement are independent. This greatly simplifies the computation of $f(\widetilde{\mathbf{X}},\mathbf{X}_b)$, which assumes the following form:

$$f(\widetilde{\mathbf{X}},\mathbf{X}_b)=\left(\prod_{i=1}^{N}\varphi_i'(\widetilde{X}_i)\right)\left(\prod_{i=1}^{N}\varphi_i(X_{b,i})\right) \tag{5}$$

where φ_i' and φ_i are the marginal pdfs of the ith component of the advective and Brownian displacements, respectively. They are both normally distributed [8,12] with pdfs:

$$\varphi_i'(\widetilde{X}_i)=\frac{1}{\sqrt{2\pi X_{ii}(t)}}\exp\left[-\frac{(\widetilde{X}_i-a_i-Ut\delta_{i1})^2}{2X_{ii}(t)}\right] \tag{6}$$

and

$$\varphi_i(X_{b,i})=\frac{1}{\sqrt{4\pi D_{d,ii}t}}\exp\left[-\frac{X_{b,i}^2}{4D_{d,ii}t}\right] \tag{7}$$

Furthermore, in Eq. (6) $X_{ii}\,i=1,\ldots,N$ are the components of the displacement variance tensor $X_{ii}(t)=\langle\widetilde{X}_i'(t;\mathbf{a})\times\widetilde{X}_i'(t;\mathbf{a})\rangle$, with $\widetilde{X}_i'=\widetilde{X}_i-\langle\widetilde{X}_i\rangle$ representing the fluctuation of the advective component of the particle trajectory around its ensemble mean. Because of the first-order approximation, the components of the velocity field and of the corresponding advective displacement, which depends linearly on them, are also normally distributed.

Despite the great attention received in stochastic theories the ensemble mean concentration, also in its volume-averaged form of Eq. (4), is a crude approximation of the actual (unknown) solute concentration, as a number of natural head gradient tracer tests have shown (e.g., [13]). A measure of the difference between actual and ensemble mean concentrations is provided by the coefficient of variation:

$$CV(C_{\Delta V})=\frac{\sigma_{C_{\Delta V}}}{\langle C_{\Delta V}\rangle} \tag{8}$$

which besides $\langle C_{\Delta V}\rangle$ requires the computation of the concentration variance:

$$\sigma^2_{C_{\Delta V}}(\mathbf{x},t)=\langle C^2_{\Delta V}(\mathbf{x},t)\rangle-\langle C_{\Delta V}(\mathbf{x},t)\rangle^2 \tag{9}$$

where the first term of the right hand side of Eq. (9) assumes the following form:

$$\langle C^2_{\Delta V}(\mathbf{x},t)\rangle=\frac{1}{\Delta V^2}\int_{\Delta V}\mathrm{d}\mathbf{x}'\int_{\Delta V}\mathrm{d}\mathbf{y}\langle C_{\Delta V}(\mathbf{x}',t)C_{\Delta V}(\mathbf{y},t)\rangle \tag{10}$$

After specializing $C_{\Delta V}(\mathbf{x},t)$ of Eq. (3) to the locations $\mathbf{x}=\mathbf{x}'$ and $\mathbf{x}=\mathbf{y}$ within ΔV and substituting the resulting expressions into Eq. (10) we obtain:

$$\langle C^2_{\Delta V}(\mathbf{x},t)\rangle=\frac{1}{\Delta V^2}\int_{\Delta V}\mathrm{d}\mathbf{x}'\int_{\Delta V}\mathrm{d}\mathbf{y}\int_{V_0}\mathrm{d}\mathbf{a}\int_{V_0}\mathrm{d}\mathbf{b}\int\mathrm{d}\widetilde{\mathbf{X}}\int\mathrm{d}\widetilde{\mathbf{Y}}\times C_0(\mathbf{a})C_0(\mathbf{b})\phi(\widetilde{\mathbf{X}},\widetilde{\mathbf{Y}},\mathbf{x}'-\widetilde{\mathbf{X}},\mathbf{y}-\widetilde{\mathbf{Y}}) \tag{11}$$

In Eq. (11) ϕ is the joint pdf of $\widetilde{\mathbf{X}}(t,\mathbf{a})$, $\widetilde{\mathbf{Y}}(t,\mathbf{b})$, $(\mathbf{x}'-\widetilde{\mathbf{X}})$ and $(\mathbf{y}-\widetilde{\mathbf{Y}})$, where we used the condition $\mathbf{x}'=\widetilde{\mathbf{X}}+\mathbf{X}_b$ and $\mathbf{y}=\widetilde{\mathbf{Y}}+\mathbf{Y}_b$ for a particle originating in $\mathbf{a}$ and $\mathbf{b}$, respectively, stemming from the property of the Dirac delta function in the Eq. (3). Owing to the independence of advective and Brownian displacements, ϕ assumes the following form:

$$\phi(\widetilde{\mathbf{X}},\widetilde{\mathbf{Y}},\mathbf{x}-\widetilde{\mathbf{X}},\mathbf{y}-\widetilde{\mathbf{Y}})=g(\widetilde{\mathbf{X}},\widetilde{\mathbf{Y}};t,\mathbf{a},\mathbf{b})\varphi(\mathbf{x}-\widetilde{\mathbf{X}})\times\varphi(\mathbf{y}-\widetilde{\mathbf{Y}}) \tag{12}$$

where g is the joint pdf of the advective components of the trajectory of two-particles simultaneously released at time $t=0$ and positions $\mathbf{x}=\mathbf{a}$ and $\mathbf{x}=\mathbf{b}$, respectively. We refer to the work of Fiori and Dagan [12] for the discussion of the hypotheses underlying Eq. (12), while here we report their conclusion that the first-order approximation of g is multivariate normal:

$$g(\widetilde{\mathbf{X}},\widetilde{\mathbf{Y}};t,\mathbf{a},\mathbf{b})=\prod_{i=1}^{N}g_i(\widetilde{X}_i,\widetilde{Y}_i;t,a_i,b_i) \tag{13}$$

where g_i is the multivariate normal pdf of the ith components of $\widetilde{\mathbf{X}}$ and $\widetilde{\mathbf{Y}}$:

$$\begin{aligned}g_i(\widetilde{X}_i,\widetilde{Y}_i;t,a_i,b_i)&=\frac{1}{2\pi\sqrt{\Xi_{ii}(t;\mathbf{a}-\mathbf{b})}}\exp\Big\{\Big[X_{ii}(t)(x_i-a_i-\delta_{1i}Ut)^2\\&\quad-2Z_{ii}(t;\mathbf{a}-\mathbf{b})(x_i-a_i-\delta_{1i}Ut)(y_i-b_i-\delta_{1i}Ut)\\&\quad+X_{ii}(t)(y_i-b_i-\delta_{1i}Ut)^2\Big]\cdot[2\Xi_{ii}(t;\mathbf{a}-\mathbf{b})]^{-1}\Big\}\end{aligned} \tag{14}$$

where $\Xi_{ii}(t;\mathbf{a}-\mathbf{b}) = X_{ii}(t)^2 - Z_{ii}(t;\mathbf{a}-\mathbf{b})^2$. Besides X_{ij}, the two-particle trajectory covariances $Z_{ij}(t;\mathbf{a}-\mathbf{b}) = \langle \widetilde{\mathbf{X}}'_i(t;\mathbf{a})\widetilde{\mathbf{Y}}'_j(t;\mathbf{b})\rangle$ are needed for computing ϕ [12].

The relative importance of PSD with respect to advection is measured by the Peclet number, which in natural formations may assume different values in longitudinal, $Pe_L = UI_{Yh}/D_{d,11}$, and transverse horizontal, $Pe_{Th} = UI_{Yh}/D_{d,22}$ and vertical $Pe_{Tv} = UI_{Yv}/D_{d,33}$, directions, where I_{Yh} and I_{Yv} are the horizontal and vertical log-conductivity integral scales, respectively. Because we address the problem in a two-dimensional domain we set $Pe_T = Pe_{Th}$, while Pe_{Tv} is inconsequential. There are experimental evidences suggesting that $Pe = \mathrm{O}(10^2) - \mathrm{O}(10^3)$ [11] with the smaller values observed in longitudinal direction. In order to explore the impact of PSD in the simulations we kept constant the transverse Peclet number to $Pe_T = 1000$ and varied the longitudinal one such as to explore the impact on concentration moments of different anisotropy ratios $R_{Pe} = Pe_T/Pe_L$. PSD enters in Eq. (14) through X_{ii} and Z_{ii}, which are influenced by mixing between streamlines. Streamline mass exchange in turn is controlled by Pe_T and is only slightly influenced by Pe_L (see [10,12] for an exhaustive treatment of this issue). Thus, the latter can be neglected in the expression of X_{ii} and Z_{ii} proposed by Fiori [10] and Fiori and Dagan [12], respectively.

The non-linear dependence of Z_{ii} on $\mathbf{a}$ and $\mathbf{b}$ prevents obtaining a closed form solution of Eq. (11). To overcome this difficulty Fiori and Dagan [12] limited themselves to injection volumes of characteristic size smaller than the log-conductivity integral scale such that $Z_{ij}(t;\mathbf{a}-\mathbf{b}) \cong Z_{ij}(t;0)$, allowing closed form solutions. Notwithstanding, we show in Section 4 that results obtained by using this simplifying assumption are accurate well beyond the formal limit of small source volume.

The computations leading to the first-order solutions of the first two moments of the solute concentration $C_{\Delta V}$ with support volume ΔV for a fully three-dimensional domain are summarized in the Appendix A.

3. Numerical simulations

In order to contain the computational effort within acceptable limits we focus on a two-dimensional formation with hydraulic log-conductivity modeled as a RSF with constant mean $\langle Y\rangle$ and variance σ_Y^2, and following an isotropic exponential covariance function:

$$C_Y(r) = \sigma_Y^2 \exp[-r/I_Y], \tag{15}$$

where r is the two-point separation distance and $I_Y = I_{Yh}$ is the log-conductivity integral scale.

We define the sampling volume ΔV as a rectangular solid of square area ΔA, which represents the sampling area, and height equal to the aquifer thickness, b. Similarly, the solute source is a volume $V_0 = A_0 b$, where A_0 is the source area. Furthermore, as shown in Fig. 1, the sampling area ΔA is square with side Δ, and the source area A_0 is

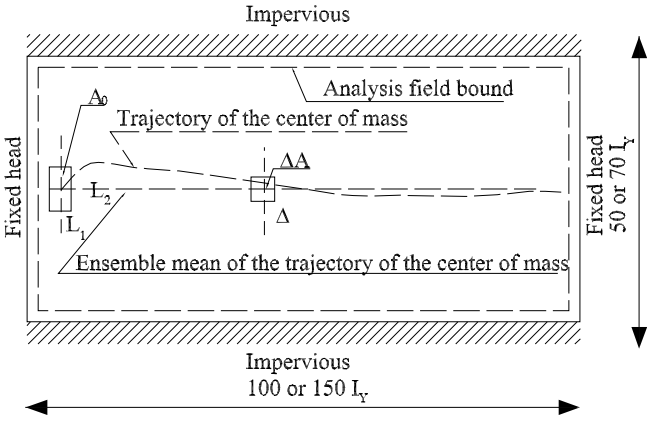

Fig. 1. Sketch of the two-dimensional computational domain.

rectangular with sides L_1 and L_2 in longitudinal and transverse directions, respectively.

To reproduce the variations of the hydraulic conductivity accurately on the computational grid, we used a square grid with side fixed at $0.25I_Y$, as suggested by Bellin et al. [5] and supported by Rubin et al. [17], who showed that the contribution of the wiped-out variability on solute spreading is negligible for block's sizes smaller than $0.25I_Y$. Flow is solved by using the Galerkin's finite element method with triangular elements and linear shape functions. The grid's block is divided into two triangles, which share the longest side and same hydraulic conductivity. Furthermore, the uniform grid's spacing leads to elements of same size, such that the maximum principle is respected everywhere within the domain, and velocity distribution is consistent with Darcy's law [15].

Transport following an instantaneous release of solute with constant concentration C_0 within the source volume V_0 is solved in a Lagrangian framework with the total solute mass, $M_0 = nC_0V_0$, partitioned into N_p particles each one of mass $\Delta m = M_0/N_\mathrm{p}$. As customary, we assume that particles travel without deformation along the trajectory of their centers of mass [18]:

$$X_{t,j}(t;\mathbf{a}) = X_{t,j}(t-\Delta t;\mathbf{a}) + V_j[\mathbf{X}_t(t-\Delta t;\mathbf{a})]\Delta t + X_{b,j}(t) \tag{16}$$

where $X_{b,j} = \sqrt{2\Delta t D_{d,jj}}\varepsilon_j$ is the jth component of the Brownian jump simulating diffusion by PSD; here $D_{d,jj}$ is jth component of the diagonal dispersion tensor, and ε_j is a random variable normally distributed with zero mean and unitary variance. Furthermore, $\mathbf{a}$ is the location where the particle is released within the source volume V_0, $V_j(\mathbf{x}) = U\delta_{1j} + u_j(\mathbf{x})$ is the jth component of the local "Eulerian" velocity field with constant mean $\mathbf{U} = (U,0)$ and fluctuation $\mathbf{u} = (u_1,u_2)$, while δ_{1j} is the Kronecker's delta.

Eq. (16) is applied recursively to all particles, and the mean concentration of the solute within the sampling volume $\Delta V = \Delta A b$ centered at the position $\mathbf{x}$ is computed as follows:

$$C_{\Delta V}(\mathbf{x},t) = \frac{n_\mathrm{p}(\mathbf{x},t)\Delta m}{n\Delta V} = \frac{C_0V_0}{\Delta V}\frac{n_\mathrm{p}(\mathbf{x},t)}{N_\mathrm{p}} \tag{17}$$

where $n_p(\mathbf{x},t)$ is the number of particles that are within the horizontal projection ΔA of the sampling volume ΔV at time t. According to this methodology, commonly known as forward particle tracking (FPT), a particle is considered either inside, or outside of ΔV, depending on the position of its center of mass. It can be shown that this procedure converges to the exact solution of the transport equation when $N_p \to \infty$.

According to Eq. (17), particle tracking results in stepwise variations of the solute concentration with discrete increment equal to $\Delta C_{\Delta V,\min} = C_0 V_0/(N_p \Delta V)$, which is also the minimum detectable concentration. Consequently, in order to maintain constant $\Delta C_{\Delta V,\min}$, a reduction of the ratio $\Delta V/V_0$ should be counterbalanced by an increase of the total number of particles (N_p). Thus, an exceedingly large number of particles is needed in order to assess point sampling accurately when the source volume is large making FPT inefficient particularly for Monte Carlo studies.

In such cases, a valuable alternative is the backward particle tracking (BPT) approach proposed by Vanderborght [19] and applied successfully in numerical simulations by Caroni and Fiorotto [6], who showed convergence of this method with the analytical solution of point concentrations for different degrees of pore-scale dispersion. The methodology consists of two steps. A given number, n_f, of solute particles are placed within the sampling volume ΔV centered at $\mathbf{x}$. Successively, each particle is moved backward in time toward the source at each time step with two successive displacements: a Brownian jump, modeled as:

$$X_j^*(t-\Delta t;\mathbf{x}) = X_{t,j}(t;\mathbf{x}) - X_{b,j} \quad j=1,2 \tag{18}$$

and an advective motion, based on the local velocity $\mathbf{V} = \mathbf{U} + \mathbf{u}$ at the position $\mathbf{x} = \mathbf{X}^*(t-\Delta t;\mathbf{x})$:

$$X_{t,j}(t-\Delta t,\mathbf{x}) = X_j^*(t-\Delta t;\mathbf{x}) - V_j[\mathbf{X}^*(t-\Delta t;\mathbf{x})]\Delta t \quad j=1,2. \tag{19}$$

If a particle changes grid element and hence velocity during the time interval Δt, its path is divided into as many subpaths as the changes in velocity and the interval is updated at each sub-step. Eqs. (18) and (19) are applied recursively to all particles. At the last step of the backward procedure the position of all particles at $t=0$ is identified and solute concentration is computed by the following equation:

$$C(\mathbf{x},t) = \frac{n_p(V_0,t)}{n_f} C_0 \tag{20}$$

where $n_p(V_0,t)$ is the number of particles inside the source volume at time $t=0$, and C_0 is the solute concentration within the source. Eq. (20) considers the fact that only the particles ending their backward path within the source area contribute to the solute concentration at time t and location $\mathbf{x}$. In this scheme the minimum detectable concentration is given by: $\Delta C_{\Delta V,\min} = C_0/n_f$, corresponding to the case when only one of the particles released within ΔV ends its journey backward in time within the source.

Notice that BPT and FPT are complementary methodologies; for a given number of particles BPT is more accurate than FPT when $\Delta V \ll V_0$, while FPT is preferable when $\Delta V \simeq V_0$, or larger. For this reason numerical results presented in this work are obtained either by using FPT or BPT depending on the ratio $\Delta V/V_0$.

4. Comparison of first-order and numerical solutions

In this section, we compare our first-order solutions of $\langle C_{\Delta V}\rangle$, $\sigma^2_{C_{\Delta V}}$ and $CV(C_{\Delta V})$ for finite sampling volume with numerical Monte Carlo simulations. We considered a square source area with side $L_1 = L_2 = L = 0.5 I_Y$ and $R_{Pe} = 10$. Additionally, we adopted a minimum detectable concentration of $6.2510^{-4} C_0$ and 2000 Monte Carlo simulations (MC), which obtained convergence of the large time $CV(C_{\Delta V})$.

Fig. 2a–c show $\langle C_{\Delta V}\rangle$, $\sigma^2_{C_{\Delta V}}$ and $CV(C_{\Delta V})$, respectively, at the center of mass of the mean plume in a weakly heterogeneous formation with $\sigma_Y^2 = 0.2$ for the following three sampling volumes: $\Delta = 0.2 I_Y$, $0.5 I_Y$ and $1 I_Y$. In addition, the corresponding first-order solutions of Fiori and Dagan [12] for point concentrations are depicted by a dashed-dot line in each one of the three plots. Our first-order solutions of both the ensemble mean and variance compare very well with the numerical simulations, as one can observe by comparing lines and symbols in Fig. 2a and 2b, respectively. Furthermore, these figures show the impact of sampling volume, which reduces the peak of both moments with respect to point concentration solutions.

An important property of a plume is ergodicity, which facilitates data interpretation and modeling because in this situation the ensemble mean concentration resembles the actual (observable) concentration. Strictly speaking ergodicity is reached when $CV(C_{\Delta V}) \to 0$, a condition that, however, is hard to obtain, as clearly shown in Fig. 2c, which compares our first-order solution of $CV(C_{\Delta V})$ (Eq. (8)) with the Monte Carlo simulations. As expected, a larger sampling volume results in a smaller $CV(C_{\Delta V})$, and our first-order solution captures this feature accurately. Fig. 2c also shows that the sampling volume has a significant impact on uncertainty affecting small plumes at short to intermediate times. At longer times since injection, the impact of the sampling volume reduces and becomes negligible for $t > 100 I_Y/U$ when convergence to ergodicity is controlled by PSD. Later in the paper, we will explore the reciprocal role of V_0 and ΔV in obtaining an operational ergodicity.

For $\Delta V = 0.2 I_Y$ the ensemble mean concentration obtained with our first-order model is in a good agreement with numerical simulations and both show small differences with the first-order solution of Fiori and Dagan [12] for point concentrations. The three solutions show a slightly larger difference when considering the concentration variance of Fig. 2b, but reduces to a level comparable to that of the ensemble mean when the coefficient of variation of Fig. 2c is considered. These results are in line with what

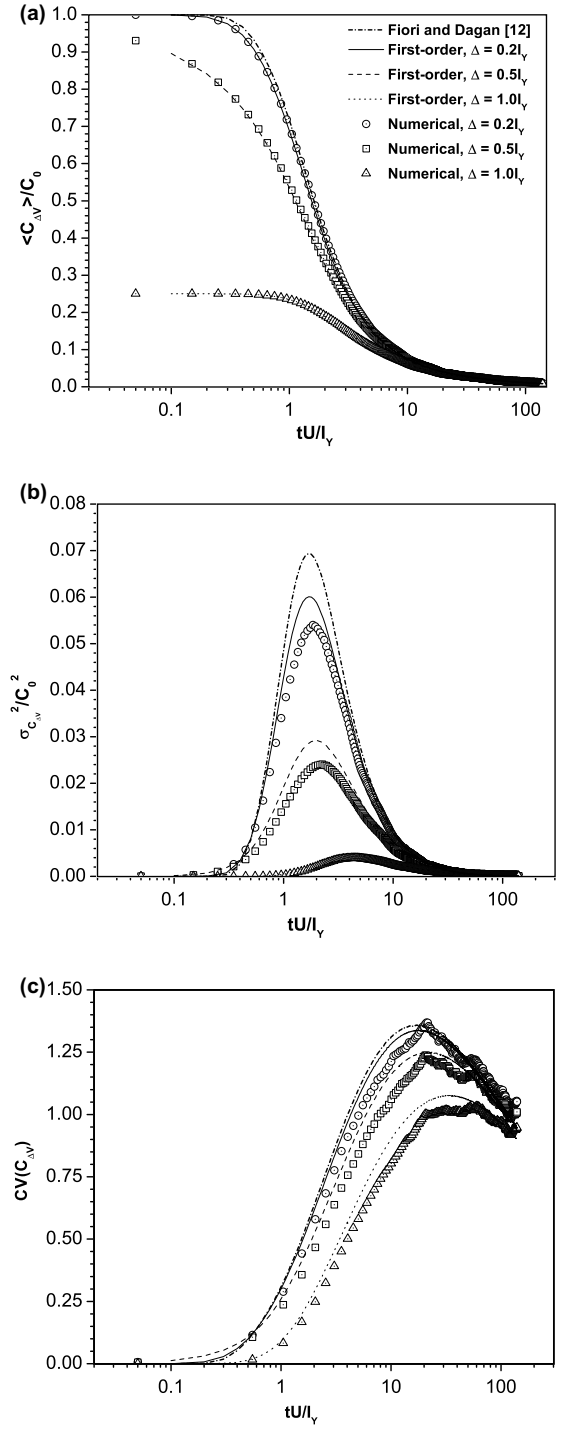

Fig. 2. First-order solutions of (a) $\langle C_{\Delta V}\rangle$ (Eq. (A.1)), (b) $\sigma^2_{C_{\Delta V}}$ (Eq. (9)), and (c) $CV(C_{\Delta V})$ (Eq. (8)) at the center of mass of the mean plume (i.e., at $\mathbf{x} = (Ut,0)$) are compared with numerical simulations (symbols) and the first-order solutions for point concentration of Fiori and Dagan [12] (dashed-dot lines). Several sampling volumes are considered and in all cases, the source area is a square with side $L = 0.5I_Y$, $\sigma^2_Y = 0.2$, $Pe_T = 1000$, and $R_{Pe} = 10$.

was previously observed by Bellin et al. [4], and suggest that if we use CV as a measure of uncertainty then point concentrations can be operationally defined as the concentration detected with a sampling device, whose size is smaller than $0.2I_Y$.

Formation heterogeneity play an important role in solute transport and in the performance of the first-order solutions. Consequently, we investigated its effect by repeating the previous simulations with increased σ^2_Y to 1. Numerical and first-order solutions are reported in Fig. 3, which shows that our models perform well also for moderate heterogeneity ($\sigma^2_Y = 1$) and capture the sampling size mixing process, which is absent in Fiori and Dagan [12] solutions. Additionally, our results show a faster decline of the ensemble mean concentration as a consequence of a stronger solute spreading due to the more complex spatial variability of the velocity field than in the previous weakly heterogeneous case. A closer inspection of Figs. 2b and 3b reveals that a larger formation heterogeneity results in an earlier and higher peak of the concentration variance, followed by a faster decline (for instance compare $\sigma^2_{C_{\Delta V}}$ values at time $t = 10\,tU/I_Y$ in Figs. 2b and 3b), due to a quicker decay of the ensemble mean concentrations.

However, the most important consequence of a larger σ^2_Y is that $CV(C_{\Delta V})$ increases dramatically and in turn also the uncertainty, as shown in Fig. 3c where the peak is roughly twice than in Fig. 2c. It is also visible that the sampling volume ΔV exerts a less intense attenuating effect on $CV(C_{\Delta V})$ than in the previous case.

So far we considered solute concentrations at the center of mass of the mean plume. To test our solution in other parts of the plume in Fig. 4 we analyze the evolution of the first two moments and the coefficient of variation of solute concentrations at the following two positions: $\mathbf{x} = (2.5I_Y,0)$ and $\mathbf{x} = (10I_Y,0)$, with the origin of the reference system at the center of the source. These two positions may be assumed as representative of resident concentrations at short and intermediate distances from the source, respectively. In Fig. 4, our first-order solutions are compared with numerical simulations for weakly heterogenous formations, i.e. $\sigma^2_Y = 0.2$ and for $R_{Pe} = 1$. Source dimensions are $L_1 = L_2 = 1I_Y$, and results are shown for both $\Delta = 0.2I_Y$ and $\Delta = 1I_Y$. At both distances from the source, our first-order solutions of $\langle C_{\Delta V}\rangle$ (Eq. (A.1)) and $\sigma^2_{C_{\Delta V}}$ (Eq. (9)) are in good agreement with numerical simulations with the maximum difference observed for $\Delta = 1I_Y$. The attenuating effect of the sampling volume on $\langle C_{\Delta V}\rangle$ is significant close to the source, but reduces with the distance and becomes small to negligible at intermediate distances. Similarly, this effect on $\sigma^2_{C_{\Delta V}}$ reduces with distance, but less rapidly than for $\langle C_{\Delta V}\rangle$. This different behavior of the first two moments is reflected to $CV(C_{\Delta V})$ shown in Fig. 4c. Notice that in Fig. 4b and a the reduction of $\sigma^2_{C_{\Delta V}}$ is partially compensated by the concomitant reduction of $\langle C_{\Delta V}\rangle$, such that only a moderate reduction of $CV(C_\Delta)$, and thus of the uncertainty, is associated with the significant enlargement of the sampling volume from $\Delta = 0.2I_Y$ to $\Delta = 1I_Y$ at both distances from the source (see Fig. 4c).

The attenuation effect of the sampling volume on $\langle C_{\Delta V}\rangle$ reduces when larger values of σ^2_Y are used, as it is shown in

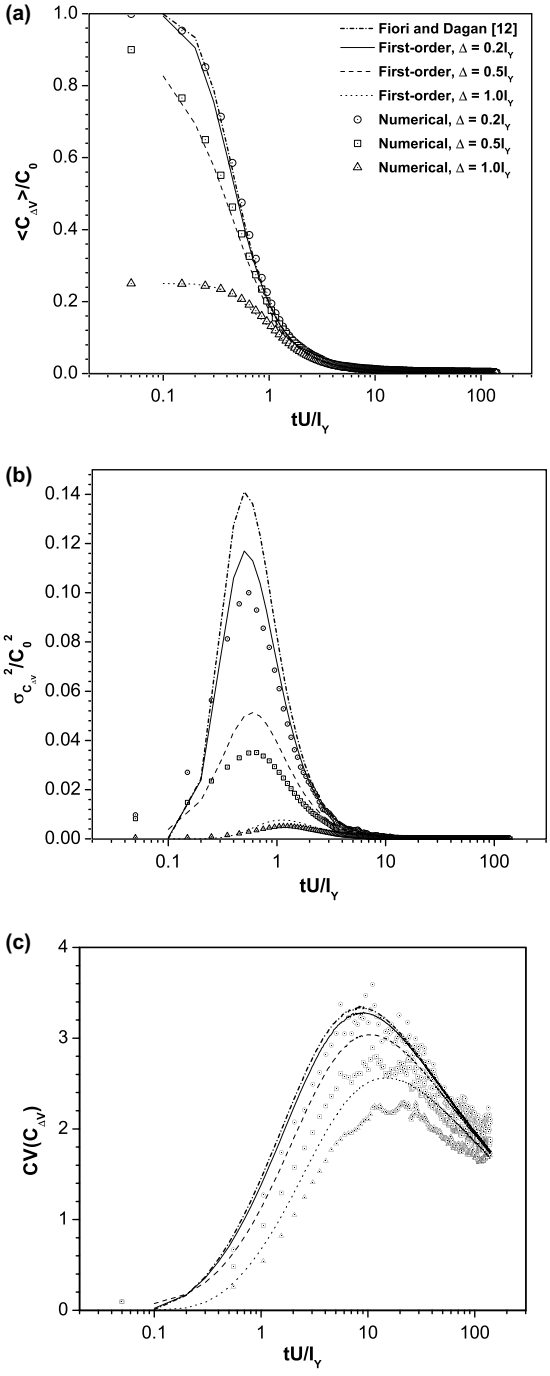

Fig. 3. First-order solutions of (a) $\langle C_{\Delta V}\rangle$ (Eq. (A.1)), (b) $\sigma^2_{C_{\Delta V}}$ (Eq. (9)), and (c) $CV(C_{\Delta V})$, (Eq. (8)) at the center of mass of the mean plume (i.e., at $\mathbf{x} = (Ut,0)$) are compared with numerical simulations (symbols) and the first-order solutions for point concentration of Fiori and Dagan [12] (dashed-dot lines). Several sampling volumes are considered and in all cases, the source area is a square with side $L = 0.5I_Y$, $\sigma^2_Y = 1$, $Pe_T = 1000$, and $R_{Pe} = 10$.

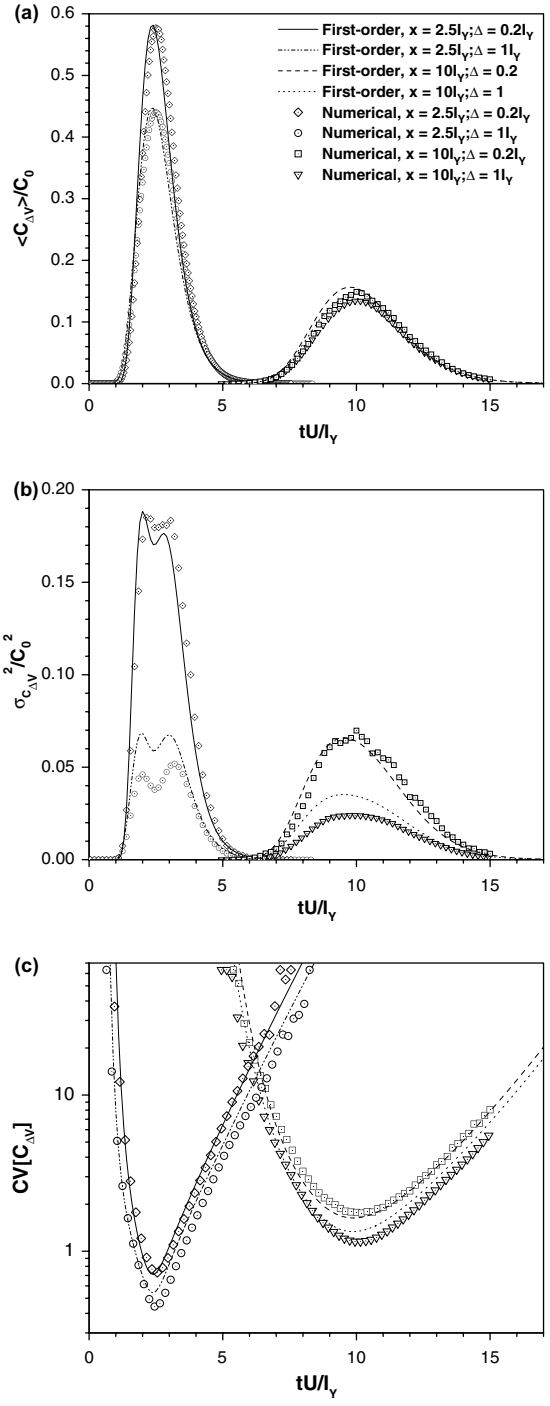

Fig. 4. First-order solutions of (a) $\langle C_{\Delta V}\rangle$ (Eq. (A.1)), (b) $\sigma^2_{C_{\Delta V}}$ (Eq. (9)), and (c) $CV(C_{\Delta V})$ (Eq. (8)) are compared with numerical simulations (symbols) at $\mathbf{x} = (2.5I_Y,0)$ and $\mathbf{x} = (10I_Y,0)$ for several sampling volumes. In all cases, the source area is a square with side $L = 1I_Y$, $\sigma^2_Y = 0.2$, $Pe_T = 1000$, and $R_{Pe} = 1$.

Fig. 5a, which is obtained with $\sigma^2_Y = 1.2$. As spreading increases with heterogeneity, solute is dispersed over a larger area faster resulting in two effects: a reduction of the smoothing effect due to mixing within the sampling volume and a lowering of the concentration peaks (c.f., Figs. 4a and 5a). For instance, Fig. 5a (numerical results) shows that the peak of $\langle C_{\Delta V}\rangle$ at $\mathbf{x} = (2.5I_Y,0)$ reduces by 6.7% when Δ is enlarged from $0.2I_Y$ to $1I_Y$, while the same enlargement produced a more pronounced reduction (i.e., 23.8%) for $\sigma^2_Y = 0.2$ (see numerical results in Fig. 4). However, a different behavior is observed for $\sigma^2_{C_{\Delta V}}$, with the

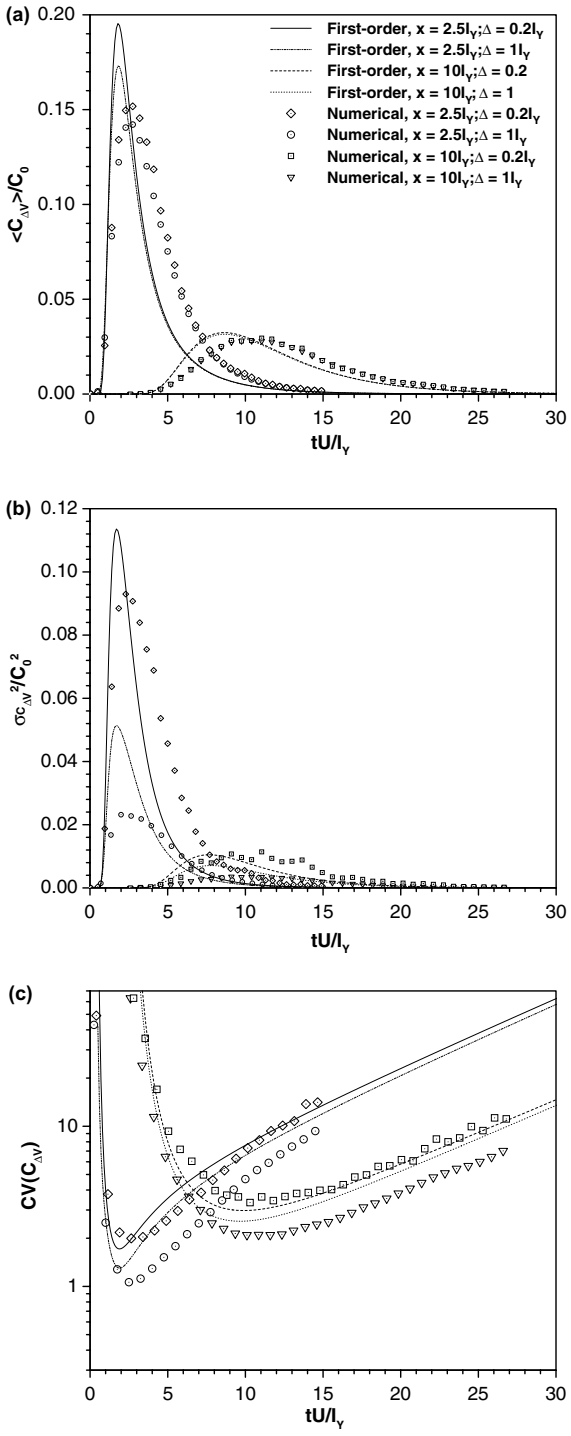

Fig. 5. First-order solutions of (a) $\langle C_{\Delta V}\rangle$ (Eq. (A.1)), (b) $\sigma^2_{C_{\Delta V}}$ (Eq. (9)), and (c) $CV(C_{\Delta V})$ (Eq. (8)) are compared with numerical simulations (symbols) at $\mathbf{x}=(2.5I_Y,0)$ and $\mathbf{x}=(10I_Y,0)$ for several sampling volumes. In all cases, the source area is a square with side $L=1I_Y$, $\sigma^2_Y=1.2$, $Pe_T=1000$, and $R_{Pe}=1$.

relative difference between the peaks for $\Delta=0.2I_Y$ and $1I_Y$ that increases from 72% to 76% when σ^2_Y is changed from 0.2 to 1.2.

On the other hand, for a given ΔV, the peaks of both $\langle C_{\Delta V}\rangle$ and $\sigma^2_{C_{\Delta V}}$ reduce progressively as σ^2_Y increases, and the aquifer becomes more heterogeneous. The drop of the concentration variance with the distance from the source is much larger for $\sigma^2_Y=1.2$ than for $\sigma^2_Y=0.2$, as emerging from an accurate inspection of Figs. 4b and 5b. In fact, the relative reduction of $\sigma^2_{C_{\Delta V}}$ between $\mathbf{x}=(2.5I_Y,0)$ and $\mathbf{x}=(10I_Y,0)$ increases from 171% for $\sigma^2_Y=0.2$ to 1000% for $\sigma^2_Y=1.2$. Solute spreading mechanisms, whose efficiency increases with higher heterogeneity, could explain this effect by anticipating the variance peak and consequently the variance decline as supported by comparing Figs. 2b and 3b. However, uncertainty depends on the coefficient of variation, which is analyzed subsequently.

The coefficient of variation shows a minimum for times comparable with the mean travel time to the observation points. Comparison of Figs. 4c and 5c shows that the case with a higher heterogeneity ($\sigma^2_Y=1.2$) has a higher minimum. Thus, a larger σ^2_Y leads to more uncertain predictions of peak solute concentrations by their ensemble mean. Additionally, $CV(C_{\Delta V})$ increases for both shorter and longer times, when the leading and trailing edges of the plume cross the observation point, as evidenced in Figs. 4c and 5c (note the use of the logarithmic scale in the ordinate axis). The behavior of $CV(C_{\Delta V})$ along the trailing edge of the plume, i.e. the tail of the resident concentration curve, differentiates the two cases. For long times since injection, the coefficient of variation shows a more gentle relative increase with time for $\sigma^2_Y=1.2$ than for $\sigma^2_Y=0.2$. As a consequence, the resident concentration curve shows a more extensive, yet less uncertain, tailing for $\sigma^2_Y=1.2$ than for $\sigma^2_Y=0.2$.

Furthermore, Fig. 5a and 5b shows that the match between numerical and our first-order solutions of $\langle C_{\Delta V}\rangle$ and $\sigma^2_{C_{\Delta V}}$ deteriorates as the aquifer becomes more heterogeneous ($\sigma^2_Y>1$). Numerical results for both $\langle C_{\Delta V}\rangle$ and $\sigma^2_{C_{\Delta V}}$ show smaller peaks and longer tailings than the corresponding first-order solutions, prolonging the persistence of solute within the sampling volume. This effect is more evident for observation points close to the source, where transport is not fully developed and the hypothesis that the particle's trajectory is Gaussian does not hold [8].

5. Effects of PSD, sampling size, and source dimension

5.1. Point concentration

Fig. 6 shows the first two moments and the coefficient of variation of point concentrations versus the source volume by increasing L from $0.1I_Y$ to $20I_Y$ with $0.1I_Y$ increments, and for the following two times: $t=10U/I_Y$ and $t=15U/I_Y$. The source volume has a square horizontal projection with side L, centered at $\mathbf{x}=(10I_Y,0)$, and extends over the entire aquifer's thickness. Concentration measurements are taken at the center of mass of the mean plume at time $t=10U/I_Y$, whereas measurements at the latter time, when the center of the mean plume is ahead (downstream) of the monitoring location at $\mathbf{x}=(10I_Y,0)$, represent sampling in a generic point within the mean plume. Solute mass was

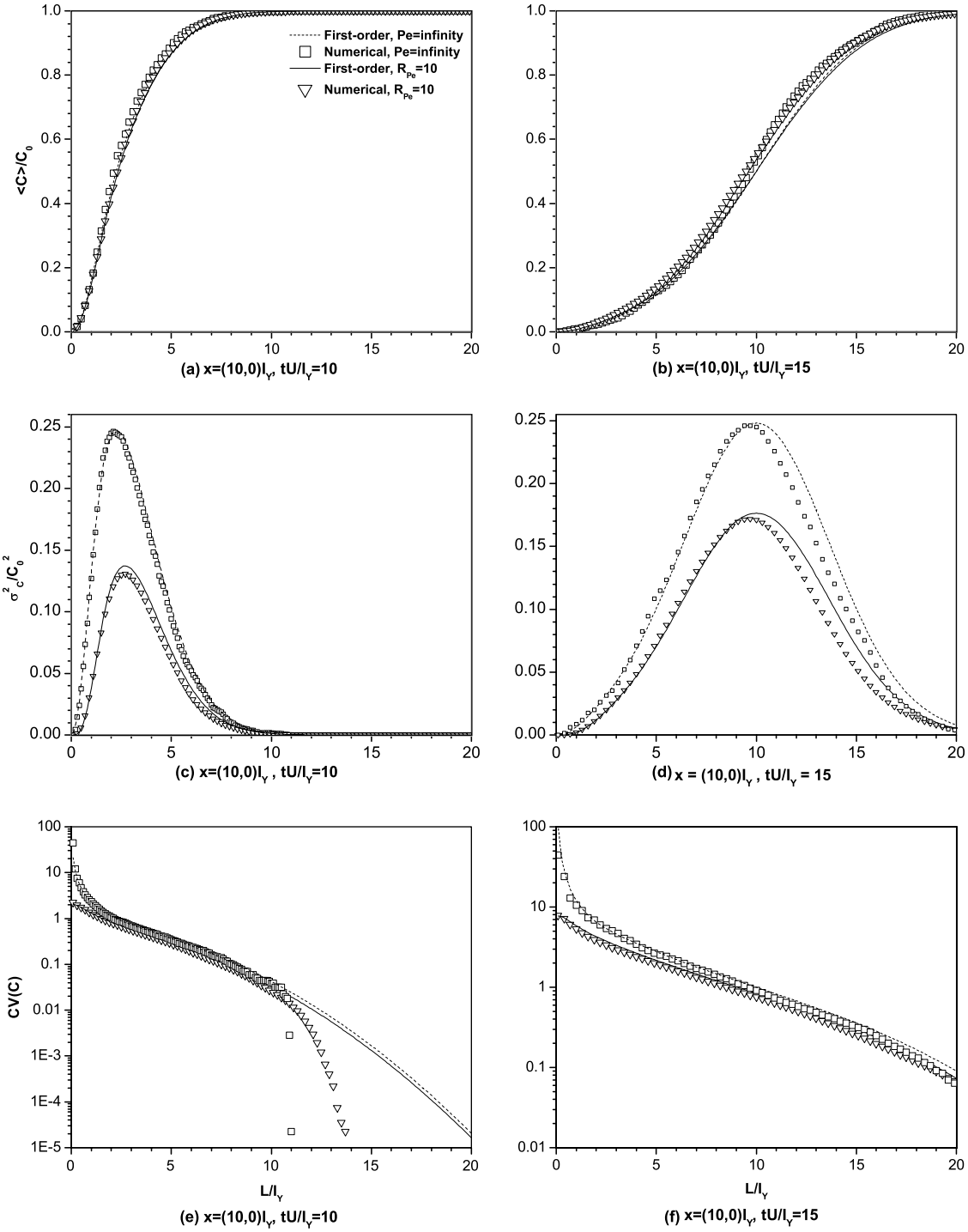

Fig. 6. First-order and numerical solutions of ensemble mean ((a) and (b)), variance ((c) and (d)), and coefficient of variation ((e) and (f)) of solute point concentrations as a function of source size at $\mathbf{x} = (10I_Y, 0)$ for $t = 10I_Y/U$ (left column) and $t = 15I_Y/U$ (right column), with $\sigma_Y^2 = 0.2$. Solutions obtained in the absence of PSD (i.e., $Pe \to \infty$) are compared with those obtained with $Pe_T = 1000$, and $R_{Pe} = 10$.

injected instantaneously and uniformly within the source volume. The influence of PSD was analyzed by comparing the concentration moments for $Pe \to \infty$ with those for $R_{Pe} = 10$ in the same graph. In all cases considered in Fig. 6, the first-order solutions of $\langle C_{\Delta V} \rangle$ (Eq. (A.1)) and $\sigma^2_{C_{\Delta V}}$ (Eq. (9)), which as shown previously for $\Delta V \to 0$ resemble the solutions for point concentration obtained by Fiori and Dagan [12], compare very well with the benchmarks provided by the numerical simulations.

What is immediately clear from Fig. 6a and b is that PSD exerts a negligible influence on the ensemble mean concentration at both times since injection as it was previously reported (e.g., [8,10]). Nevertheless, it causes a significant reduction of the concentration variance as shown in

Fig. 6c and d. The striking result shown in these two figures is that the first-order solution is accurate beyond its formal limit of applicability for small source volume, i.e. $L \ll I_Y$, resulting from assuming $Z_{ii}(t;\mathbf{a}-\mathbf{b}) \simeq Z_{ii}(t;0)$; $i=1,2$ in Eq. (18) of Fiori and Dagan [12].

As expected $CV(C)$ decreases with source size reaching an operational (source size induced) ergodicity when $CV(C) \to 0$ for large L. However, this limit is not obtained for the same source size everywhere within the plume. In fact, $CV(C)$ decreases to zero more rapidly at the center of mass of the plume, where concentrations are expected to be the highest, than in other positions, as shown in Fig. 6e and f. Notice that the drop of the numerical solution in Fig. 6e for $L/I_Y > 10$ is an artifact due to the impossibility of measuring concentrations below the detectable limit associated with the elementary mass of the particle. We run a simulation with double number of particles and the outcome shows that the numerical solution drops at a higher L. Since we are not interested in analyzing situations with CV smaller than the one where the drop occurs in Fig. 6e we do not increase the number of particles, which would have caused a much higher computational effort.

Because in all the above comparisons with $\sigma_Y^2 < 1$ our first-order solutions are in a good agreement with the benchmark numerical simulations also with large source sizes, we investigate the interplay among source size, sampling volume, and PSD with our first-order solutions in the remaining of this paper without showing their numerical counterparts.

5.2. Volume-averaged concentration

We analyzed the effect of both source and sampling volumes on the concentration moments at $\mathbf{x}=(10I_Y,0)$ by increasing Δ from $0.05I_Y$ to $5I_Y$ with $0.05I_Y$ increments and the source volume as described above. Source and sampling volumes have a square horizontal projection with side L and Δ, respectively, and both extend over the entire aquifer's thickness. Like in the previous simulations, solute mass was injected instantaneously and uniformly within the source volume.

We present the influence of Δ and L on $\langle C_{\Delta V}\rangle$ at $\mathbf{x}=(10I_Y,0)$ in Fig. 7a and b, obtained for $t=10I_Y/U$ and $t=150\ I_Y/U$, respectively. Additionally, in the same figures we compare $\langle C_{\Delta V}\rangle$ solutions predicted with ($R_{Pe}=10$) and without PSD (i.e., $Pe\to\infty$). Source size is the major factor controlling $\langle C_{\Delta V}\rangle$, as shown by the nearly vertical contour lines in Fig. 7a and b, while PSD has a weak influence and sampling dimension plays a more important, yet minor role. The latter result was expected, since the solutions for different Δ values coalesce at $t > 10I_Y/U$ in Figs. 2 and 3 and at distances of the order of $10I_Y$ from the source in Figs. 4 and 5.

We can explain these results from a physical point of view as follows. Dilution associated with PSD and mixing within the sampling volume both contribute to attenuate the spatial variability of the solute concentration. However, since PSD acts at scales of the order of centimeters (the Darcy's scale), its influence on $\langle C_{\Delta V}\rangle$ is marginal with respect to mixing when Δ is larger than a few centimeters, i.e. a small fraction of I_Y, ($\Delta > \ell$).

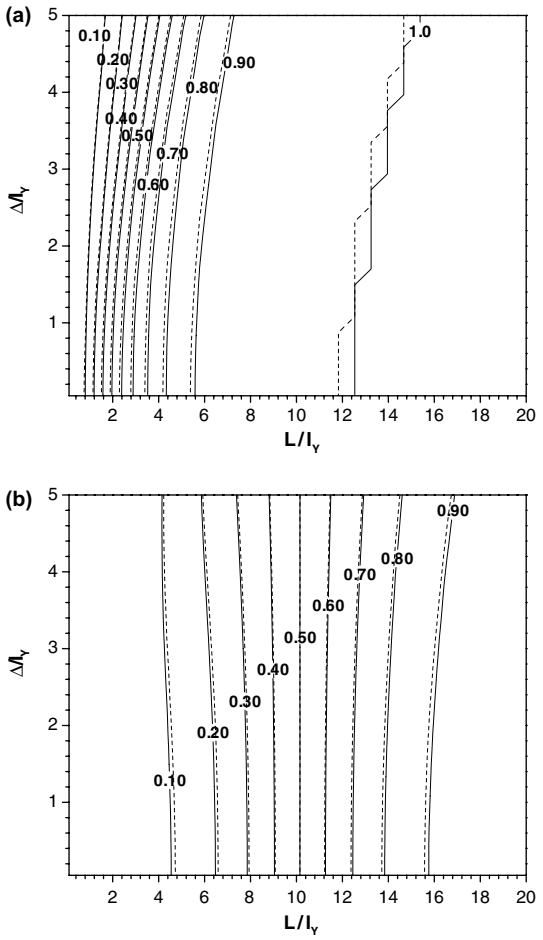

Fig. 7. Contour plot of $\langle C_{\Delta V}\rangle$ as a function of source and sampling volumes at $\mathbf{x}=(10I_Y,0)$ for (a) $t=10\ I_Y/U$ and (b) $t=15I_Y/U$, with $\sigma_Y^2=0.2$. First-order solutions obtained with $Pe_T=1000$, and $R_{Pe}=10$ (solid lines) are compared with those obtained in the absence of PSD ($Pe\to\infty$, dashed lines).

The concentration variance is expected to be much more sensitive to PSD, but the overwhelming effect of large mixing volumes may mask the PSD effect also for $\sigma^2_{C_{\Delta V}}$. Fig. 8a shows our first-order solution of $\sigma^2_{C_{\Delta V}}$ (Eq. (9)) with ($R_{Pe}=10$) and without PSD (i.e., $Pe\to\infty$) at $\mathbf{x}=(10I_Y,0)$ and for $t=10I_Y/U$. In addition, Fig. 8b replicates Fig. 8a but for $t=15I_Y/U$. We observe that a change of PSD to values typically encountered in applications (i.e., $Pe\approx \mathrm{O}(10^2)-\ \mathrm{O}(10^3)$) from the idealized case that neglects PSD (i.e., $Pe\to\infty$), causes the concentration variance to reduce noticeably at small ΔV and negligibly at large ΔV, as one would expect, because in the latter case mixing within the sampling volume exerts an overwhelming smoothing effect on the solute concentration with respect to PSD. However, source volume acts differently at $t=10I_Y/U$ and $t=15I_Y/U$, because higher variance values occur at different locations in the Δ–L plane. This is the

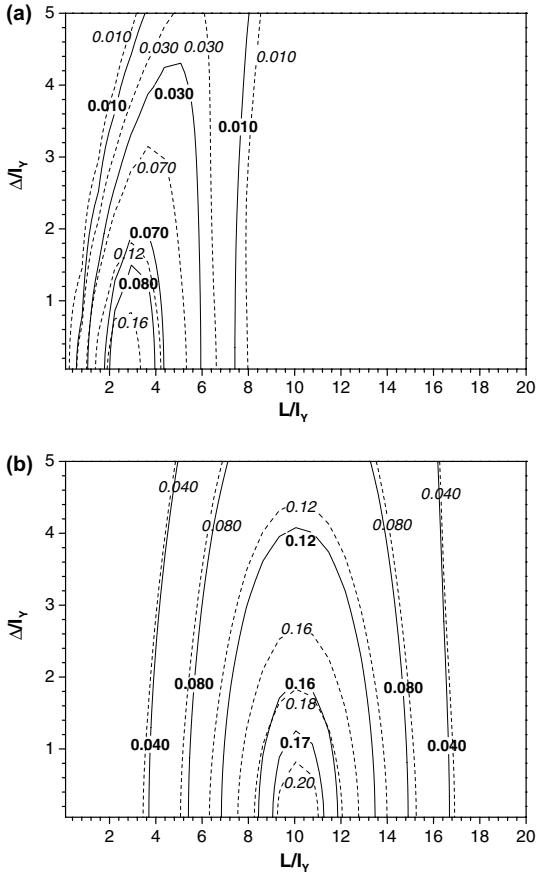

Fig. 8. Contour plot of $\sigma^2_{C_{\Delta V}}$ as a function of source and sampling volumes at $\mathbf{x} = (10I_Y, 0)$ for (a) $t = 10\ I_Y/U$ and (b) $t = 15I_Y/U$, with $\sigma^2_Y = 0.2$. First-order solutions obtained with $Pe_T = 1000$, and $R_{Pe} = 10$ (solid lines) are compared with those obtained in the absence of PSD ($Pe \to \infty$, dashed lines).

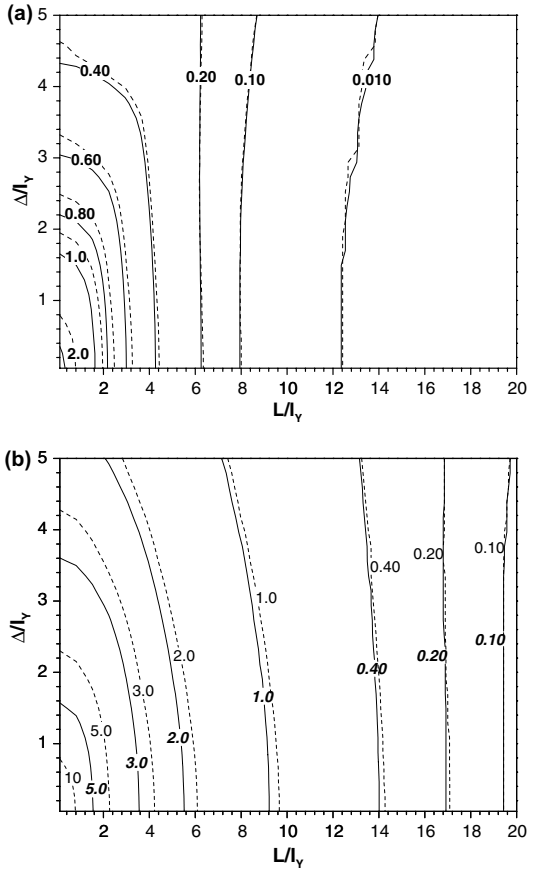

Fig. 9. Contour plots of $CV(C_{\Delta V})$ as a function of source and sampling volumes at $\mathbf{x} = (10I_Y, 0)$ for (a) $t = 10I_Y/U$ and (b) $t = 15I_Y/U$, with $\sigma^2_Y = 0.2$. First-order solutions obtained with $Pe_T = 1000$, and $R_{Pe} = 10$ (solid lines) are compared with those obtained in the absence of PSD ($Pe \to \infty$, dashed lines).

consequence of the fact that the effect of PSD is more significant where the concentration gradients are large, and this happens particularly in areas surrounding the positions where $\langle C_{\Delta V} \rangle \simeq 0.5 C_0$.

Furthermore, the most distinct feature of the concentration variance contour plot is a "ridge" that follows the contour line $\langle C_{\Delta V} \rangle = 0.5 C_0$ in the Δ–L plane of Fig. 7. Along this ridge, PSD plays a strong effect on the concentration variance, but it fades with sampling size. Because of this ridge, a given value of $\sigma^2_{C_{\Delta V}}$ can be obtained with several combinations of Δ and L. Therefore, our results evidence the interplay between source and sampling volume and strengthen the importance of knowing both in order to compute the concentration variance accurately.

Additionally, as shown in Fig. 9a and b, $CV(C_{\Delta V})$ is controlled by L and except for small source volumes (i.e., $L < 4I_Y$), with a very limited effect of Δ. Uncertainty reduces fast with sampling size at small source volumes, but at a rate that declines with increasing of source size. In addition, PSD exerts a noticeable effect on $CV(C_{\Delta V})$ at small sources, which, however, fades as the source volume grows large. Additionally, we can observe sampler-induced ergodicity at small sources and source-induced ergodicity in both plots.

5.3. Point versus volume-averaged concentrations

Because volume-averaged concentrations are the most common in applications, it is important to know their deviation from point measurements, which in turn are the most important for biological and ecological analysis. This is because microorganisms are in contact with local concentrations, whose intensity may vary from volume-averaged measurements. A measure of this difference (between volume-averaged and point concentrations) is provided by the following two quantities: $R_C = \langle C_{\Delta V} \rangle / \langle C \rangle$, and $R_{CV} = CV(C_{\Delta V})/CV(C)$. Note that values of both ratios larger than unity denote larger volume-averaged than point quantities, whereas the inverse is true for values less than 1.

Fig. 10a depicts R_C for $t = 10U/I_Y$ at $\mathbf{x} = (10I_Y, 0)$. Solid contour lines are for finite Peclet values ($R_{Pe} = 10$) and dashed lines are obtained neglecting pore-scale dispersion (i.e., $Pe \to \infty$). As expected, pore-scale dispersion exerts a negligible impact on R_C, which is controlled by both L and Δ. Notice that the smallest R_C values are observed

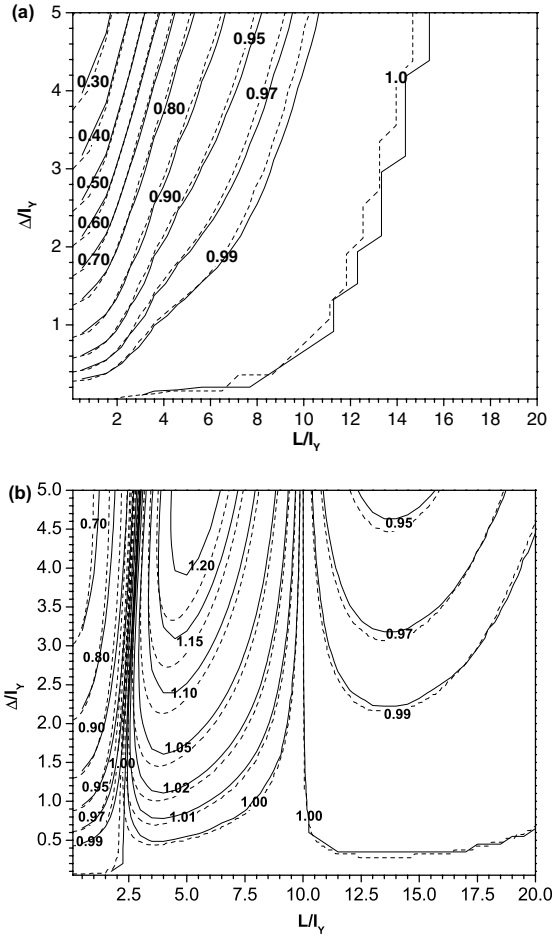

Fig. 10. Contour plots of R_C at $\mathbf{x} = (10I_Y, 0)$ for (a) $t = 10I_Y/U$ and (b) $t = 15I_Y/U$. First-order solutions obtained with $Pe_T = 1000$, and $R_{Pe} = 10$ (solid lines) are compared with those obtained in the absence of PSD ($Pe \to \infty$, dashed lines). In all cases $\sigma_Y^2 = 0.2$.

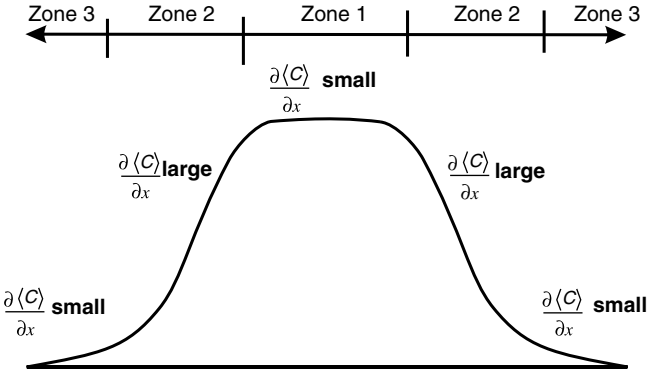

Fig. 11. Sketch of the three zones characterizing the concentration attenuation within the mean plume.

when a small plume is sampled with a large sampling volume (the left upper corner of Fig. 10a), and that R_C increases much rapidly with L for small rather than large Δ values. Furthermore, the ensemble mean of point and volume-averaged concentrations show relative differences smaller than 1% (i.e., $R_C \geqslant 0.99$) for $\Delta < L/4$, and smaller than 20% for $\Delta < L$. In other words, significant differences between the ensemble mean of point and volume-averaged concentrations are observed when $\Delta > L$.

Fig. 10b shows R_C for $t = 15U/I_Y$ and all other quantities unchanged. This figure shows that R_C can assume values either smaller or larger than 1 depending on the location of the measurement point with respect to the center of mass of the mean plume, and the interplay between Δ and L. This behavior of R_C measured at a generic point within the mean plume can be attributed to the change in rate of spatial attenuation of $\langle C \rangle$ (Fig. 11). By considering the mean plume at a given time, one can observe that the rate of attenuation of $\langle C \rangle$ first increases with distance from the center of mass, reaches the maximum value at intermediate distances (zone 2 in Fig. 11), and then declines slowly to zero as the distance from the center of mass grows large (zone 3 in Fig. 11). Based on these observations, we identify three zones: zone 1, which denotes the volume surrounding the center of mass of the mean plume with the slowest attenuation rate and whose extension depends on L, zone 2, which contains the volume with the highest concentration reduction, and zone 3, which comprises the remaining volume (Fig. 11). Therefore, R_C may be either larger or smaller than one depending on where the sampling volume falls in among these three zones. In particular, $R_C > 1$ when ΔV is sampling partially in zone 2 and 3, while $R_C < 1$ when ΔV is between zone 2 and 1 or entirely in zone 3. Furthermore, $R_C \approx 1$ when ΔV falls entirely within zone 1, owing to the small variability of the solute concentration within this zone, or zone 2, due to the constant decline of the solute concentration.

The streaking result shown in Fig. 10b is that $\langle C_{\Delta V} \rangle$ can be larger than $\langle C \rangle$ when ΔV is large enough to collect solute mass in zone 2 and 3. However, Fig. 10a shows that at the center of mass of the mean plume $\langle C_{\Delta V} \rangle \leqslant \langle C \rangle$ as one would expect. Nevertheless, because this is the location with the highest probability of observing high concentrations, we conclude that the sampling volume introduces a considerable attenuation effect on the maximum concentration with important consequence for risk analysis.

In Fig. 12, we investigated R_C at the center of mass of the mean plume as a function of time for $L = 10I_Y$ and two sampling volumes; one with $\Delta = 2I_Y$ and the other with $\Delta = 5I_Y$ corresponding to $\Delta/L = 0.2$ and 0.5, respectively. Our results show that the influence of Δ varies with time and is more pronounced for larger Δ. At early times when the sampling volume is fully inside zone 1, $R_C = 1$, but as time increases, macrodispersion acts reducing the extension of zone 1 such that R_C reduces progressively. As larger portions of the sampling device fall in zone 2, R_C reaches a minimum at intermediate travel times and then it increases as effect of the homogenization of C over larger volumes caused by solute spreading. At later times, R_C reaches a relative maximum and then it decreases again. Note that the position of the minimum is independent on sampler size, which instead controls the absolute value.

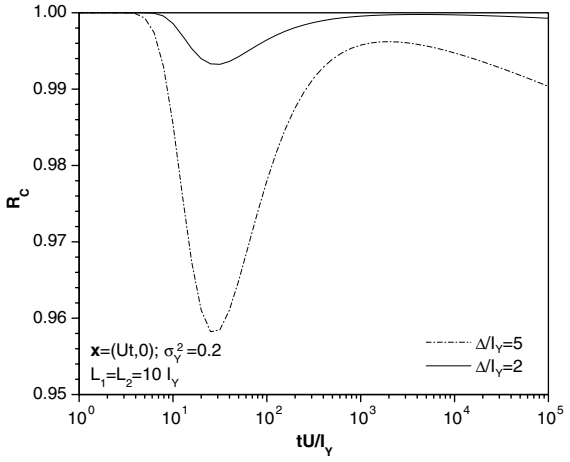

Fig. 12. R_C at the center of mass of the mean plume as a function of time and for $\Delta = 2I_Y$ and $5I_Y$. The source area is a square with side $L = 10I_Y$ and $\sigma_Y^2 = 0.2$.

In the previous sections, we analyzed how uncertainty in solute concentration, quantified by $CV(C_{DV})$, is influenced by Δ, PSD and source size. In Fig. 13 we present their combined effect on the ratio $R_{CV} = CV(C_{\Delta V})/CV(C)$ between the coefficients of variation of volume-averaged and point concentrations at $\mathbf{x} = (10I_Y,0)$ for both $t = 10U/I_Y$ and $t = 15U/I_Y$. Fig. 13a and b are obtained with $R_{Pe} = 10$, while Fig. 13c and 13d are obtained in the absence of PSD. Pair comparisons of Fig. 13a with c and b with d suggest that the influence of the sampling volume on R_{CV} depends on measurement location with respect to the expected position of the center of mass besides on source size and PSD.

Let us first focus on the case with pure advection ($Pe \to \infty$). At the center of the mean plume (Fig. 13a), an increase of Δ causes R_{CV} to decrease for small sources (let say $L < 6I_Y$), and to increase for large sources (let say $L > 6I_Y$). The latter result suggests that uncertainty are higher for volume-averaged than point concentrations at large source sizes. This has important consequences in risk analysis, because point concentration uncertainty does not always provide an upper limit. Therefore, it is important to take into account sampler and source sizes in assessing solute exposure in applications. However, CV values are small in these cases as shown in Fig. 9a.

On the other hand as shown in Fig. 13c, for a location outside the center of the mean plume (for $t = 15I_Y/U$, i.e. when the sampling volume is ahead of the expected position of the center of mass) an increase of Δ leads always (except for very large sampler and source sizes) to a reduction of R_{CV}, and this reduction attenuates with L.

In Fig. 13b and d we show the effect of PSD, which causes an attenuation of the differences between volume-averaged

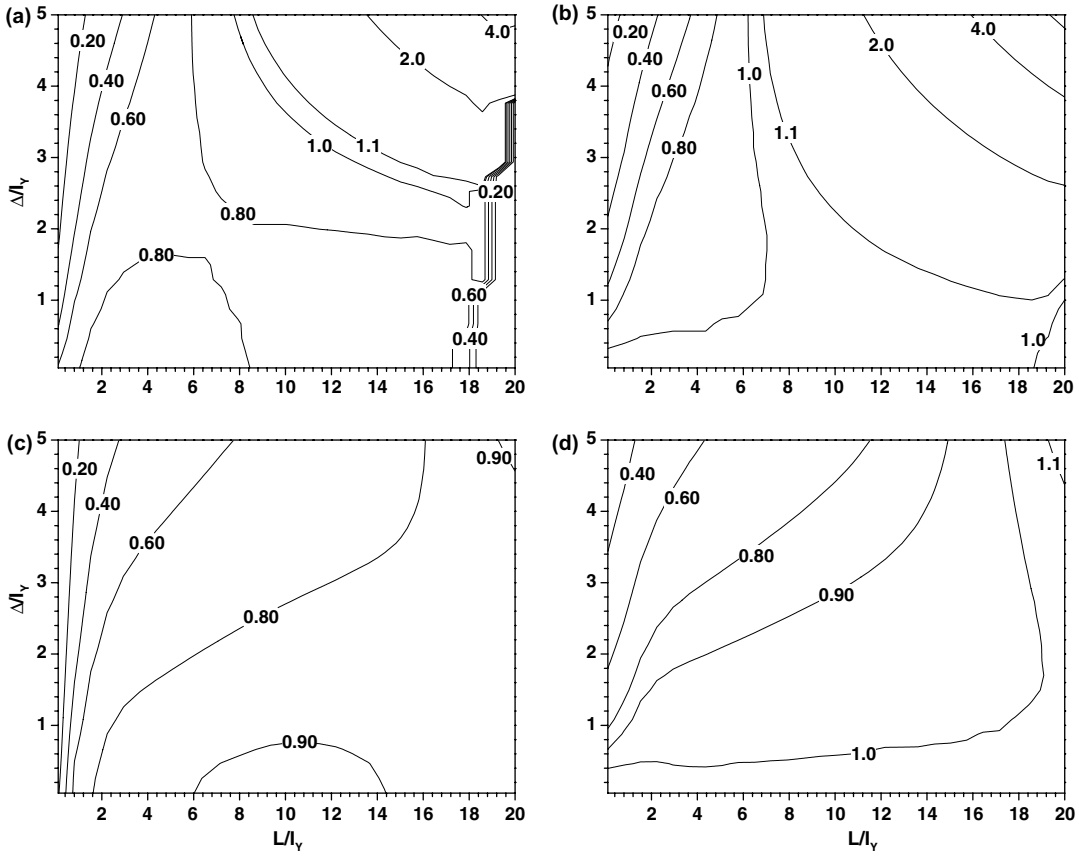

Fig. 13. Contour plots of R_{CV} at $\mathbf{x} = (10I_Y,0)$ for (a) $t = 10I_Y/U$ and $Pe \to \infty$, (b) $t = 10I_Y/U$, $Pe_T = 1000$, and $R_{Pe} = 10$, (c) $t = 15I_Y/U$ and $Pe \to \infty$, and (d) $t = 15I_Y/U$, $Pe_T = 1000$, and $R_{Pe} = 10$. In all cases $\sigma_Y^2 = 0.2$.

and point concentration coefficients of variation. However, its effect on R_{CV} is a function of sampler and source sizes as shown in Fig. 13b and d. PSD maintains $R_{CV} \approx 1$ at small sampler sizes (e.g., $\Delta < 0.2I_Y$), because of its smoothing mechanism that attenuates concentration spatial fluctuations. However, at larger Δ its effect may fade or reverse depending on source size. At small source sizes (e.g., $L < 6$ I_Y), as the sampler size increases PSD effect fades disappearing at large sampling sizes, thereby leaving the sampler size as the major controlling factor. On the other hand, at large source and large sampling volumes PSD causes an increased difference of R_{CV} from unity and R_{CV} grows larger than 1 as observed previously. Therefore, the overall effect of PSD is of reducing the difference between $CV(C_{\Delta V})$ and $CV(C)$, with the exception of large source and sampling volumes, for which PSD leads to larger uncertainty in volume averaged solute concentrations. (right-up corner of Fig. 13a and b and of c and d).

6. Conclusions

Ground water is an important resource and its careful quality management depends on water concentration analysis. However, concentration measurements are strongly dependent on the choice of the support volume (Δ) especially as sampler size grows larger than the Darcy's scale ℓ. Additionally, source size (L), pore-scale dispersion (PSD), and aquifer heterogeneity (σ_Y^2) affect concentration moments.

Therefore, our first-order solutions of concentration ensemble mean, variance, and coefficient of variation are important tools in performing concentration analysis, because they account for all these factors. An important outcome of our analysis is that applicability of our models is not limited to small sources, despite their derivation under the limiting condition of $L \to 0$. Additionally, comparison between numerical and first-order solutions shows that our model performance is accurate up to moderate heterogeneity of the formation hydraulic properties (i.e. $\sigma_Y^2 = 1$) and then decreases with aquifer heterogeneity ($\sigma_Y^2 > 1.2$).

Our analysis reveals a complex interplay among sampler size, source volume, and PSD, whose relative importance is also a function of time since injection and aquifer heterogeneity. Sampler volume smoothing effect on the concentration first moment depends on the measurement location with respect to the mean plume center and the interplay between sampler and source volume. Whereas, mixing within the sampler's volume always exerts an attenuating effect at the center of the mean plume, this is not always true in a generic point within the plume, where concentrations may be larger for volume-averaged than for point measurements. However in all cases, sampling effect fades with source size and time since injection. This is accelerated by an increase of formation heterogeneity, which attenuates the concentration first moment strongly, but increases concentration uncertainties at the center of the mean plume. However, concentration uncertainties (CV) may decrease with larger σ_Y^2 at the plume fringe.

Additionally, source size has a paramount influence on the mixing effect of the sampler volume on concentration uncertainty. At the center of the mean plume, the coefficient of variation decreases rapidly with sampler volume at small source size. However as source size increases, this effect fades and eventually reverses causing concentration uncertainty to increase with sampling size. Notwithstanding, sampler volume causes a decrease of CV for other locations around the center of the mean plume except for very large source and sampling volumes.

Furthermore, we suggest that sampler size mechanism might be enhanced in a three-dimensional field as water is captured and mixed from different elevations. On the other hand, its effect should decrease faster with distance or time since injection, because as the plume spreads within the aquifer, it samples the formation heterogeneity more efficiently [9]. Another, factor, which we did not analyze in this work, but might affect the relative importance of PSD, sampler, and source volume is source shape, which has been shown to influence concentration moments (e.g., [1]). However, we hypothesize that source shape should not change the outcome of our analysis, but it could probably anticipate or postpone the onset of one factor's influence.

Nevertheless, as time passes pore-scale dispersion, which acts at a scale much smaller than the sampler volume mixing mechanism, starts influencing solute concentration moments. Whereas, PSD has a negligible effect on ensemble mean solute concentrations regardless of source and sampling dimensions, it attenuates concentration variance and thus reduces uncertainty plaguing analyses based on the evolution of ensemble mean concentrations. Additionally, PSD has another beneficial effect by reducing the difference between point and volume-averaged CVs. However, its influence fades quickly with sampler size. It is important to notice that PSD effect on the difference between point and volume-averaged concentration CVs reverses for very large source and sampler sizes causing volume-averaged measurements to have higher uncertainty.

As last remarks, we summarize the following 4 findings for the zone around the plume center of mass, which comprises the highest solute concentrations and thus bear important information in risk assessment:

(1) At short times since injection, and as long as $\Delta \ll L$, the main factor controlling concentration distribution is the sampling volume, with pore-scale dispersion and source size both playing a minor role.
(2) Source size should be considered when it is of the same order or smaller than the sampling size ($L \leqslant \Delta$), and both sampling volume dimension and PSD play an equal important role.
(3) At long times since injection, which may be the case for old contaminations, PSD introduces an appreciable additional smoothing to the concentration, while sampling volume plays a minor role.

(4) Increases of aquifer heterogeneity causes a reduction of the ensemble mean concentration, but an increase in uncertainty.

Acknowledgements

We would like to thank Daniel Fernandez-Garcia and five anonymous reviewers for their insightful and careful reviews. The second author acknowledges the support of the European Commission through the project AquaTerra (contract no. 505428).

Appendix A. Ensemble mean and variance of passive solute concentrations

We consider a two- or three-dimensional formation with hydraulic property variations described by a geostatistical model of spatial variability epitomized through the mean, variance and covariance function of the hydraulic log-conductivity (or log-transmissivity in the case of a two-dimensional regional model). Pore-scale dispersion is parameterized through the longitudinal $Pe_L = UI_{Yh}/D_{d,11}$ and transverse horizontal $Pe_{Th} = UI_{Yh}/D_{d,22}$ and vertical $Pe_{Tv} = UI_{Yv}/D_{d,33}$ Peclet numbers. For a two-dimensional formation only the longitudinal and horizontal transverse Peclet numbers are defined. Notice that our results are not limited to these two models of spatial variability, and other geostatistical models can be utilized provided that the moments X_{ii} and Z_{ii} are available.

By substituting Eq. (5) of the joint probability distribution of $\widetilde{\mathbf{X}}$ and $\mathbf{X}_b$ into Eq. (4) we obtain, after integration, the following expression for $\langle C_{\Delta V}\rangle$ (Eq. (4)):

$$\frac{\langle C_{\Delta V}(\mathbf{x},t)\rangle}{C_0} = \prod_{i=1}^{N} I_{ii}(x_i,t) \tag{A.1}$$

where the functions I_{ii}, $i = 1, \ldots, N$ are given by

$$\begin{aligned} I_{ii}(x_i,t) = \frac{1}{L_i}\Bigg\{\frac{1}{4}\Bigg[&(2x_i - \Delta_i + L_i - 2\delta_{i1}t)\\ &\cdot \operatorname{erf}\left[\frac{\Delta_i - L_i - 2x_i + 2\delta_{i1}t}{2\sqrt{2X_{t,ii}(t)}}\right] + (\Delta_i + L_i - 2x_i + 2\delta_{i1}t)\\ &\cdot \operatorname{erf}\left[\frac{\Delta_i + L_i - 2x_i + 2\delta_{i1}t}{2\sqrt{2X_{t,ii}(t)}}\right] - (2x_i + \Delta_i - L_i - 2\delta_{i1}t)\\ &\cdot \operatorname{erf}\left[\frac{\Delta_i - L_i + 2x_i - 2\delta_{i1}t}{2\sqrt{2X_{t,ii}(t)}}\right] + (2x_i + \Delta_i + L_i - 2\delta_{i1}t)\\ &\cdot \operatorname{erf}\left[\frac{\Delta_i + L_i + 2x_i - 2\delta_{i1}t}{2\sqrt{2X_{t,ii}(t)}}\right]\Bigg] + \sqrt{\frac{X_{t,ii}(t)}{2\pi}}\\ &\times\Bigg[-\exp\left[-\frac{(\Delta_i - L_i + 2\delta_{i1}t - 2x_i)}{8X_{t,ii}(t)}\right]\\ &+\exp\left[-\frac{(\Delta_i + L_i + 2\delta_{i1}t - 2x_i)}{8X_{t,ii}(t)}\right]\\ &-\exp\left[-\frac{(\Delta_i - L_i - 2\delta_{i1}t + 2x_i)}{8X_{t,ii}(t)}\right]\\ &+\exp\left[-\frac{(\Delta_i + L_i - 2\delta_{i1}t + 2x_i)}{8X_{t,ii}(t)}\right]\Bigg]\Bigg\} \end{aligned} \tag{A.2}$$

In Eq. (A.2), $X_{t,ii}(t) = X_{ii}(t) + 2D_{d,ii}t$ is the total displacement variance. Notice that as shown by Fiori [10] X_{ij} is influenced by the transverse Peclet numbers (i.e. Pe_{Th} and Pe_{Tv} for the three-dimensional case and $Pe_T = Pe_{Th}$ for the two-dimensional case) and only slightly by Pe_L, which is then neglected in the expression of X_{ii}. The source and the sampling volume have dimensions L_i, and Δ_i $i = 1,2,3$, respectively, in the three-dimensional case. In the two-dimensional case the source is rectangular with sides L_i, $i = 1,2$ and extending over the aquifer thickness b. The sampling volume is also of thickness b with dimensions Δ_i, $i = 1,2$ in the horizontal plane. As shown in Fig. 1 the subscript "1" refers to quantities measured along the mean flow direction. Furthermore, in Eq. (A.2) lengths are dimensionless with respect to the log-conductivity integral scale I_{Yh}, time t with respect to I_{Yh}/U, and particles displacement variances $X_{t,ii}$ with respect to I_{Yh}^2. In the absence of pore-scale dispersion Eq. (A.1) specialized to the two-dimensional case resembles the first-order solution obtained by Bellin et al. [4].

We consider now $\sigma^2_{C_{\Delta V}}$, which according to Eq. (9) can be decomposed into two components. We also assume that Z_{ii} is independent from the releasing points of the particles. Under this simplifying assumption and after substituting Eq. (12) into Eq. (11), and integrating the resulting expression, we obtain:

$$\begin{aligned} \langle C^2_{\Delta V}(\mathbf{x},t)\rangle = &\frac{C_0^2}{\left(\prod_{i=1}^{N}\Delta_i\right)^2}\prod_{i=1}^{N}\int_{x_i-\Delta_i/2}^{x_i+\Delta_i/2}\mathrm{d}r\\ &\times\int_{-L_i/2}^{L_i/2}\mathrm{d}a_i\Theta(r,a_i) \end{aligned} \tag{A.3}$$

where the function $\Theta(r,a_i)$ is given by

$$\begin{aligned} \Theta(r,a_i) = &\frac{1}{2\sqrt{2\pi X_{t,ii}(t)}}\exp\left[-\frac{(r-\delta_{i1}t-a_i)^2}{2X_{t,ii}(t)}\right]\\ &\times[G_i(\gamma_i, x_i+\Delta_i/2) - G_i(\gamma_i, x_i-\Delta_i/2)\\ &-G_i(\alpha_i, x_i+\Delta_i/2) + G_i(\alpha_i, x_i-\Delta_i/2)] \end{aligned} \tag{A.4}$$

with

$$G_i(\zeta,s) = \frac{\mathrm{e}^{-(\zeta-s\beta_i)^2}}{\sqrt{\pi}\beta_i} + \left(s - \frac{\zeta}{\beta_i}\right)\operatorname{erf}(s\beta_i - \zeta) \tag{A.5}$$

Finally, the functions α_i, β_i and γ_i are given by

$$\alpha_i = \beta_i\left[\frac{L_i}{2} + \delta_{i1}t + (r - \delta_{i1}t - a_i)\frac{Z_{ii}(t;0)}{X_{t,ii}(t)}\right] \tag{A.6}$$

$$\beta_i = \frac{X_{t,ii}(t)}{\sqrt{2X_{t,ii}(t)(X_{t,ii}(t)^2 - Z_{ii}(t;0)^2)}} \tag{A.7}$$

$$\gamma_i = \alpha_i - L_i\beta_i \tag{A.8}$$

Inspection of Eqs. (A.1) and (9) reveals that for vanishing ΔV, both $\langle C_{\Delta V} \rangle$ and $\sigma^2_{C_{\Delta V}}$ converge to the expressions proposed by Fiori and Dagan [12].

References

[1] Andričević R. Effects of local dispersion and sampling volume on the evolution of concentration fluctuations in aquifers. Water Resour Res 1998;34(5):1115–29.

[2] Batchelor GK. An Introduction to fluid dynamics. Cambridge: Cambridge University Press; 1967.

[3] Bear J. Dynamics of fluids in porous media. New York: Elsevier Science; 1972.

[4] Bellin A, Rubin Y, Rinaldo A. Eulerian-Lagrangian approach for modeling of flow and transport in heterogeneous geological formations. Water Resour Res 1994;30(11):2913–24.

[5] Bellin A, Salandin P, Rinaldo A. Simulation of dispersion in heterogeneous porous formations: Statistics, first-order theories, convergence of computations. Water Resour Res 1992;28(9): 2211–27.

[6] Caroni E, Fiorotto V. Analysis of concentration as sampled in natural aquifers. Transp Porous Media 2005;59:19–45.

[7] Dagan G. Flow and transport in porous formations. New York: Springer-Verlag; 1989.

[8] Dagan G, Fiori A. The influence of pore-scale dispersion on concentration statistical moments in transport through heterogeneous aquifers. Water Resour Res 1997;33(7):1595–605.

[9] Fernàndez-Garcia D, Illangasekare TH, Rajaram H. Differences in the scale dependence of dispersivity and retardation factors estimated from forced-gradient and uniform flow tracer tests in a three-dimensional physically and chemically heterogeneous porous media. Water Resour Res 2005;41(W03012).

[10] Fiori A. Finite-Peclet extensions of Dagan's solutions to transport in anisotropic heterogeneous formations. Water Resour Res 1996;32(1): 193–8.

[11] Fiori A. The relative dispersion and mixing of passive solutes in transport in geologic media. Transport in Porous Media 2000;42:69–83.

[12] Fiori A, Dagan G. Concentration fluctuations in aquifer transport: A rigorous first-order solution and applications. J Contam Hydrol 2000;45(1-2):139–63.

[13] Fitts CR. Uncertainty in deterministic groundwater transport models due to the assumption of macrodispersive mixing: evidence from Cape Cod (MA, USA) and Borden (Ontario, Canada) tracer tests. J Contam Hydrol 1996;23:69–84.

[14] Gelhar LW. Stochastic subsurface hydrology. Englewood Cliffs, NJ: Prentice Hall; 1993.

[15] Putti M, Cordes C. Finite element approximation of the diffusion operator on tetrahedra. SIAM J Sci Stat Comp 1998;19:1154–68.

[16] Rubin Y. Applied Stochastic Hydrogeology. New York: Oxford University Press; 2003.

[17] Rubin Y, Sun A, Maxwell R, Bellin A. The concept of block-effective macrodispersivity and a unified approach for grid-scale- and plume-scale-dependent transport. J Fluid Mech 1999;395:161–80.

[18] Tompson AFB, Gelhar LW. Numerical simulation of solute transport in three-dimensional, randomly heterogeneous porous media. Water Resour Res 1990;26(10):2451–562.

[19] Vanderborght J. Concentration variance and spatial covariance in second-order stationary heterogeneous conductivity fields. Water Resour Res 2001;37(7):1893–912.

[20] Zhang D, Neuman SP. Effect of local dispersion on solute transport in randomly heterogeneous media. Water Resour Res 1996;32(9): 2715–23.